THE ASTROPHYSICAL JOURNAL, 358:298–312, 1990 July 20

NUCLEAR LINE SPECTROSCOPY OF THE 1981 APRIL 27 SOLAR FLARE

R. J. MURPHY[1] AND G. H. SHARE
E. O. Hulburt Center for Space Research, Naval Research Laboratory
J. R. LETAW
Severn Communications Corporation
AND
D. J. FORREST
Department of Physics and Astronomy, University of New Hampshire
Received 1989 July 31; accepted 1990 January 17

ABSTRACT

We present the details of a quasi–model-independent analysis technique for determining the intensities, line centers, and widths of the narrow gamma-ray lines appearing in observed count spectra from solar flares. We apply the technique to observations of the 1981 April 27 solar flare obtained with the gamma-ray spectrometer on board the *Solar Maximum Mission* spacecraft. To obtain an acceptable fit to the data, we find that the assumed shape of the underlying continuum used in the model must have considerably more structure than simple shapes can provide. This additional structure is required to account for nuclear gamma-ray emission other than that appearing in narrow lines. We find also that, while the derived line centers are well determined, the best-fit values of both the intensities and widths of the narrow lines can vary appreciably as the assumed underlying continuum model is changed. Using a continuum model which closely approximates the continuum expected from solar flares on the basis of theoretical considerations, we also investigate how the total emission attributed to electron interactions and the emission attributed to nuclear interactions varied as the flare progressed. These total emissions should be relatively free of the uncertainties affecting the narrow lines. We find that, while the intensities of both of these emissions varied considerably, their ratio was consistent with a constant value throughout the flare. The near-constancy of this ratio suggests that the associated nuclei and electrons in this flare were accelerated by common or related mechanisms. The results obtained here for the 1981 April 27 flare form a baseline with which results from other flares can be compared when their data are analyzed in a similar manner. The technique provides a simple and efficient tool for the statistical analysis of data from a large number of flares.

Subject headings: gamma rays: general — radiation mechanisms — Sun: flares

I. INTRODUCTION

The shapes and relative intensities of the various narrow and broad lines present in solar flare gamma-ray spectra can provide information on the acceleration and interaction processes occurring in solar flares and on the nature of the interaction region itself. For example, line shapes can reveal the angular distribution of the interacting accelerated particles (see Murphy, Kozlovsky, and Ramaty 1988; Murphy *et al.* 1990), and line intensities can reveal the composition of both the ambient solar atmosphere (see Murphy *et al.* 1985*a*, *b*) and the accelerated particles. Providing spectral information that can be used by the solar physics community is a fundamental task for observers of solar flares. A major challenge in deriving believable line parameters (i.e., the line intensities, central energies, and widths) is the reliable determination of the level and spectral shape of the underlying continuum. For solar flares this continuum is composed of electron bremsstrahlung (which is essentially featureless) plus a "nuclear continuum" (possessing weak structure). Also, since observations of gamma-ray spectra are obtained in the form of pulse-height count distributions of energy-loss spectra, there is an additional continuum of counts due to escape of Compton-scattered photons from the detector. This latter continuum can be effectively "removed" with a detailed and accurate model of the response of the detector to gamma rays of various energies. The former continuum, however, is intrinsic to the gamma-ray source itself, and its treatment becomes a critical part of the fitting procedure used to determine the parameters.

In this paper we determine the intensities, central energies, and widths of the 13 strongest narrow lines appearing in the pulse-height count spectrum obtained with the *Solar Maximum Mission* (*SMM*) satellite gamma-ray spectrometer (GRS) from the 1981 April 27 solar flare. All parameter values are simultaneously optimized by fitting over the entire usable energy range (0.3–8.5 MeV) of the GRS. (This method has been applied to the analysis of the *SMM*/GRS spectrum from the Earth's atmosphere by Letaw *et al.* 1989.) The sensitivity of the derived narrow-line parameters to the underlying continuum is tested by assuming different continuum shapes and refitting the lines. We also determine how the total emissions attributed to nuclear interactions and to electron interactions vary as the flare progresses.

Gamma-ray production in solar flares is discussed in some detail in § II; this discussion provides theoretical background information so that a continuum model can be developed which has the detail required to provide a good fit to the data. The detection of gamma rays is reviewed in § III, and the 1981 April 27 solar flare data are described in § IV. The analysis

[1] Resident Research Associate at the Naval Research Laboratory under the NRC Associateship Program.

technique used here is discussed in § V, along with a brief description of previous spectroscopic analyses of these same data. In § VI the results of applying the technique to the April 27 data are presented and compared with those of previous analyses of this flare. We summarize in § VII. A discussion of the estimation of uncertainties associated with derived parameters is included in an appendix.

II. GAMMA-RAY PRODUCTION IN SOLAR FLARES

The sudden release of energy in a solar flare results in the acceleration of charged particles (electrons, protons, and heavier nuclei). These particles may then interact with the ambient solar atmosphere to produce both gamma rays (e.g., relativistic electron bremsstrahlung) and a variety of secondary products which may also produce gamma rays. The bremsstrahlung of relativistic electrons is observable as gamma-ray continuum. At energies below ~ 1 MeV, this emission dominates and the spectrum is typically observed to be a power law. This spectral shape may continue to higher energies, but above ~ 1 MeV the contribution from the nuclear secondaries becomes important and masks that of the electrons.

The most important of the secondary nuclear products are neutrons, excited and radioactive nuclei, and π-mesons. Neutrons may be captured by H at the Sun and produce the 2.22 MeV neutron-capture gamma-ray line. Gamma-ray lines are also produced by the de-excitation of various nuclei (at a number of line energies) and by the annihilation of positrons (at 0.51 MeV). The excited nuclei are produced both by inelastic excitation reactions and by spallation reactions involving heavier nuclei. The positrons result from decay of the radioactive nuclei and of charged π-mesons. The decay of neutral π-mesons leads to high-energy ($\gtrsim 30$ MeV) broad-band gamma-ray emission.

The strongest de-excitation lines expected from solar flares are at 6.129 MeV from ^{16}O, 4.439 MeV from ^{12}C, 2.313 MeV from ^{14}N, 1.779 MeV from ^{28}Si, 1.634 MeV from ^{20}Ne, 1.369 MeV from ^{24}Mg, 0.847 and 1.238 MeV from ^{56}Fe, and 0.478 and 0.429 MeV from ^{7}Li and ^{7}Be. (These last two rare isotopes, essentially absent in the solar atmosphere, result from α-particle interactions with ^{4}He.) The line energies given above are the rest-frame values but would also be observed in the laboratory frame if the angular distribution of the interacting accelerated particles were isotropic. However, other angular distributions could result in Doppler shifting of the line centers (e.g., see Ramaty and Crannell 1976; Kozlovsky and Ramaty 1977; Murphy, Kozlovsky, and Ramaty 1988). The extent of the shift depends on the angular distribution, the accelerated-particle kinetic energy spectrum, and the viewing angle.

For typical solar flare accelerated-particle energy spectra, the excited nuclei responsible for the above lines are produced predominantly by inelastic excitation rather than spallation of heavier elements (except, of course, ^{7}Li and ^{7}Be, which result from nonthermal α-α fusion). The various cross sections for inelastic excitation have similar energy dependences, and the relative intensities of the lines are therefore fairly insensitive to changes in the accelerated-particle energy spectrum. For typical solar flare accelerated-particle spectra, the fractional contribution of spallation reactions to a given line varies from zero for lines from Fe (elements heavier than Fe are insignificantly abundant in the Sun) to more than 30% for the 4.439 MeV line from ^{12}C. Since the cross sections for spallation reactions typically have higher thresholds and extend to higher energies than those for inelastic excitation, the spallation fraction generally increases as the particle spectrum hardens. As a result, these reactions can affect the line ratios when the spectrum is very hard. For a given particle spectrum, the relative intensities of de-excitation lines depend directly on the composition of either the ambient medium or the accelerated particles, depending on whether the line is narrow or broad, as discussed below.

Gamma-ray lines are produced with a variety of widths. Most of the secondary neutrons which do not escape from the Sun or decay at the Sun are captured either on ^{1}H (leading to the 2.22 MeV gamma ray) or on ^{3}He (radiationless). Since the probability for elastic scattering is much larger than that for capture, most neutrons are thermalized before being captured, leading to a very narrow line (full width at half-maximum [FWHM] $\lesssim 100$ eV) whose center energy is at the rest-frame value of 2.223 MeV. This neutron-capture line is the most intense line produced in solar flares, but the flux can be significantly attenuated by Compton scattering in the photosphere when the flare is observed to occur on the solar limb.

The majority of the positrons also thermalize and form positronium via charge exchange with neutral hydrogen before annihilation. This results in a 0.51 MeV line whose width is generally less than 10 keV and a 3 photon positronium continuum at energies below 0.51 MeV. The line center is expected to be at the rest-frame annihilation energy of 0.511 MeV.

De-excitation of nuclei produces both narrow and broad lines. If an accelerated proton or α-particle interacts with an ambient heavy nucleus (a "direct" reaction), the resultant gamma-ray line is narrow (fractional FWHM $\lesssim 2\%$ for isotropic accelerated particles), Doppler-broadened only by the relatively small recoil velocity of the heavy excited nucleus. If the accelerated particles are collimated into a beam, the line width can be narrower (by $\sim 20\%$). (The FWHM of the ~ 0.45 MeV α-α feature is about 100 keV for isotropic interactions, but this is due to blending of the two lines at 0.478 and 0.429 MeV.) Since the α-particle–to–proton ratio in the accelerated particles is typically less than 0.4, narrow lines are produced predominantly by accelerated protons and so, for a given accelerated-particle energy spectrum, the relative intensities of these lines depend only on the relative abundances of the elements in the ambient interaction medium. However, since the excited nucleus responsible for a narrow line can be produced by inelastic excitation of that nucleus in the ambient medium and by spallation of heavier nuclei, knowledge only of the relative narrow-line intensities is insufficient for directly determining relative ambient abundances.

If an accelerated heavy nucleus interacts with an ambient H or He nucleus (an "inverse" reaction), the line is very broad (fractional FWHM $\simeq 20\%$ for isotropic accelerated particles), Doppler-broadened by the velocity of the excited nucleus, which has lost little of its initial kinetic energy in the interaction. The broad lines merge into a relatively featureless "continuum" whose overall structure is directly determined by the composition of the accelerated particles.

The width of a narrow line produced by inelastic excitation is only weakly dependent on the accelerated-particle energy spectrum, since the cross sections for such excitations are generally sharply peaked. Since the cross sections for spallation reactions usually have higher thresholds and extend to higher energies, the associated lines have somewhat broader widths, which are sensitive to the particle spectrum. The widths of lines which have a strong spallation component can therefore have some spectral dependence.

In addition to the strong narrow lines mentioned above, nuclear reactions involving nuclei heavier than oxygen also produce a large number of relatively weak, closely spaced narrow lines. These lines are generally not resolved by NaI detectors (such as the *SMM*/GRS) and so effectively merge into a smooth continuum. The combination of these unresolved lines and the inverse-reaction broad lines discussed above will be referred to as the "nuclear continuum" to distinguish it from the continuum due to electron bremsstrahlung. The relative importance of the unresolved component and the broad-line component depends on the composition of both the ambient and the accelerated particles.

The various components of a solar flare nuclear de-excitation gamma-ray spectrum can be seen in Figure 1. These theoretical spectra were calculated using the Monte Carlo technique developed by Ramaty, Kozlovsky, and Lingenfelter (1979) that incorporates laboratory measurements of the energy- and angle-dependent cross sections for a large number of reactions and takes into account Doppler shifts and relativistic beaming. (The small-scale fluctuations present in the figure are due to Monte Carlo statistics.) The calculation assumed thick-target interactions (e.g., see Ramaty and Murphy 1987) and the best-fitting ambient composition obtained by Murphy *et al.* (1985*a*, *b*) for the 1981 April 27 flare. For the accelerated particles, a composition similar to that of solar flare energetic particles given by Meyer (1985) was assumed and a Bessel function kinetic energy spectrum ($\alpha T = 0.025$; e.g., see Ramaty and Murphy 1987) and an isotropic angular distribution were used. The accelerated-particle spectrum was normalized to 1 proton with energy greater than 30 MeV, and the photons were binned into 25 keV intervals. The lowest curve at lower energies is the broad component resulting from the "inverse" reactions. The weak structure present is due to interactions of accelerated Fe (at $\sim$0.85 MeV), Mg and Ne (at $\sim$1.5 MeV), C (at $\sim$4.4 MeV), and O (at $\sim$6 MeV). The next curve is an approximation of the unresolved component, composed of weak, narrow lines from nuclei heavier than O, and is relatively structureless except for the broad peak at $\sim$1–2 MeV. The sum of these two curves represents the total "nuclear continuum." For this set of assumed abundances, the unresolved component is stronger below $\sim$4 MeV, while the inverse component is stronger above $\sim$4 MeV. The total "nuclear continuum" retains some of the structure of the inverse component. The upper curve is the total nuclear spectrum, which is the sum of the total "nuclear continuum" and the narrow lines. The spectrum shows the characteristic falloff of nuclear gamma-ray emission above $\sim$8 MeV. The excited nuclei responsible for some of the strongest narrow lines are indicated.

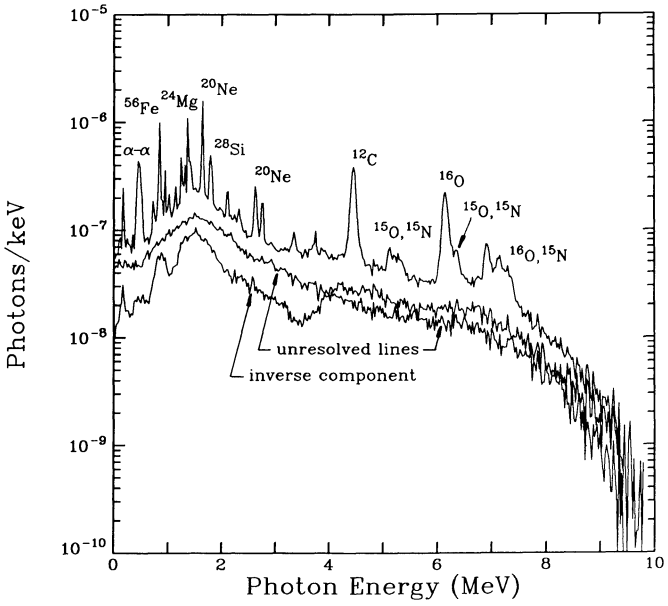

FIG. 1.—Theoretical solar flare nuclear de-excitation gamma-ray spectrum

III. GAMMA-RAY DETECTION

The *Solar Maximum Mission* gamma-ray spectrometer is an actively shielded (CsI), seven crystal, NaI scintillation detector designed to measure the flux of solar flare gamma rays. A 476 channel pulse-height count distribution of the energy-loss spectrum is produced every 16.384 s over the energy range 0.24–9.0 MeV with an energy resolution of $\sim$7% at 662 keV. The gain of each detector is continuously corrected to a common value by a feedback loop consisting of three ^{60}Co on-board calibration sources and the output of the pulse-height analyzer. Since the detectors have a common gain, their outputs are simply summed and digitized with the common pulse-height analyzer. The seven detectors are covered with an Al-Pb filter with 50% transmission at 250 keV to minimize X-ray pulse pileup and gain-shift effects. The energy-dependent effective area for line detection varies from 20 to 200 cm^{-2}, and the detector has a typical narrow-line sensitivity of $\sim 10^{-3}$ photons cm^{-2} s^{-1}. The instrument is described in more detail by Forrest *et al.* (1980).

A scintillation detector such as the *SMM*/GRS determines the energy deposited by an incident gamma-ray photon by measurement of the charge pulse it produces, the magnitude of the pulse being proportional to the energy deposited. Gamma rays interact with the detector material and deposit energy via some or all of the three dominant interaction processes: photoelectric, Compton scattering, and pair production. The energy deposited may be all or only some fraction of the original photon energy. If all of the photon energy is deposited, a count is added to that pulse-height bin whose associated energy equals the total initial photon energy (the "photopeak"). If, as the energy-loss process is occurring, a residual photon with degraded energy escapes from the detector but deposits some of its energy in the surrounding CsI shield, the event is vetoed. However, if this escaping residual photon is not detected by the shield, the event is not vetoed and a count appears in a bin corresponding only to the amount of energy that was deposited in the NaI detector. Even if every photon that interacts in the detector were to deposit all of its energy, the statistical nature of the detection process would still spread the counts across a number of bins, reducing the detector's ability to resolve closely spaced lines.

The total effect of these processes is to smear the incident photon spectrum so that direct comparison with a theoretical photon spectrum is impossible. A numerical model of the instrument response is therefore required to analyze any spectral observations. Such a model has been constructed, derived from both detector calibrations and Monte Carlo calculations, that takes into account the detector's energy-dependent effective area, resolution, photopeak, and escape peak fractions and Compton-continuum spectrum. The effects of uncertainties in the detector model parameters have been investigated and found to be negligible in the energy range of $\sim$0.3 to $\sim$7 MeV.

During the small but finite amount of time required for the data-acquisition system to process an individual gamma-ray event, the detectors are not sensitive to additional incoming gamma rays. As a result, the number of processed events in a given time interval is, in general, less than the actual number of photons interacting in the detectors. The detector electronics provide an estimate of the time during which the detector was not processing events (the "live time") which can be used to correct the observed number of counts. All photon fluxes and fluences (time-integrated fluxes) reported here and all count rates appearing in the figures have been corrected for this effect. However, the count spectra appearing in the figures have not.

IV. DESCRIPTION OF THE DATA

Solar flare pulse-height count distributions obtained with a detector in Earth orbit contain a significant number of counts due to a gamma-ray background. The primary sources of this background are gamma rays from the Earth's atmosphere and from radioactive decay of isotopes generated within the spacecraft by cosmic-ray or geomagnetically trapped particles. An accurate estimation of this background is crucial for extracting the spectrum of the flare itself. This background has been investigated extensively in general and for the *SMM*/GRS specifically (Share *et al.* 1989).

The technique developed for removing the background contribution in *SMM*/GRS solar flare data is essentially an "on-off source" approach. Count distributions are obtained 24 hours before and after a solar flare, shifted in time a small amount to reproduce as closely as possible the geomagnetic condition and spacecraft orientation that occurred during the time of the flare. These two spectra are then averaged and subtracted from the spectrum obtained during the flare. The extent to which this technique is successful has been tested by obtaining background in this manner for a period during which no flare occurred. The resulting background-subtracted spectrum was found to be consistent with zero counts in all channels.

The flare on 1981 April 27 began at about 08:04 UT and was located on the west limb of the Sun at 16° N, 90° W. The flare was a long-duration event with significant emission lasting more than 30 minutes. The time profile of the background-subtracted count rate in the 4.1–6.4 MeV energy band is shown in Figure 2. Three well-defined maxima can be seen with intervening minima followed by lower-level extended emission. Background-subtracted spectra were obtained with 16.384 s time resolution throughout the flare, and these data were then integrated over various time intervals for spectral analysis. For the full flare, the interval was 08:04:00.841 to 08:35:57.769 UT with a total detector live time of 1722.134 s (corresponding to a fractional live time of 89.8%). To search for temporal changes in the derived spectral parameters, three maximum-emission intervals were defined: 08:07:33.833 to 08:09:44.905 UT (P1), 08:12:45.129 to 08:15:12.585 UT (P2), and 08:16:50.889 to 08:18:12.809 UT (P3). Three minimum-emission intervals were also defined: 08:09:44.905 to 08:12:45.129 UT (V1), 08:15:12.585 to 08:16:50.889 UT (V2), and 08:18:12.809 to 08:20:56.649 UT (V3). These intervals are shown in Figure 2. The live times for the three maximum periods and the three minimum periods were 116.01, 132.75, 73.69, 163.87, 89.33, and 148.99 s, respectively.

During the spectrum-fitting procedure (described below), only the data in channels 11 (corresponding to 0.3 MeV) through 459 (8.5 MeV) were used. The detector response to photons with energy less than ~0.3 MeV is uncertain, while the counts above channel 459 are not statistically significant.

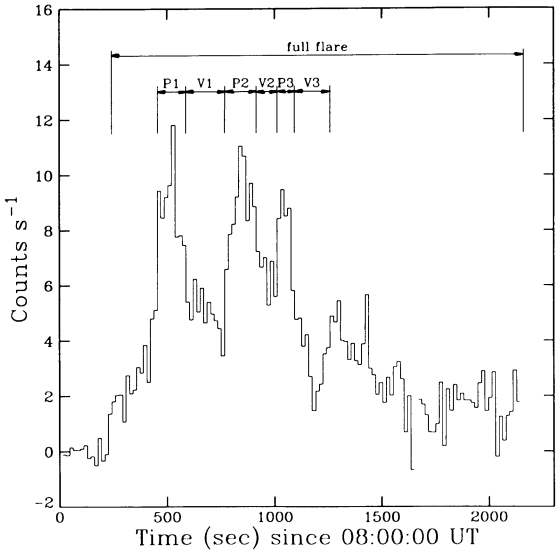

FIG. 2.—Time profile of the background-subtracted 4.1–6.4 MeV count rate from the 1981 April 27 flare.

V. ANALYSIS TECHNIQUE

a) Fitting Procedure

An observed pulse-height count distribution is a convolution of the incident photon spectrum with the instrumental response. In general, recovery of the incident spectrum is accomplished by one of two methods. In one method, the incident spectrum is obtained by "deconvolving" the count distribution, utilizing some type of inversion or maximum-entropy technique. A second method, and the method that is used here, is a "hypothesis-testing" approach in which a trial incident spectrum is constructed, is convolved with a numerical model of the instrumental response, and the resulting data function tested to determine whether it is compatible with the observed data, given their uncertainties. Such an approach is not capable of finding the unique spectrum which gave rise to the data; rather, it can only reject those spectra which could not. There is an essential danger in such an approach; that is, significantly different trial photon spectra can give rise to data functions which differ very little, each giving statistically equivalent qualities of fit (e.g., see Craig and Brown 1986). This weakness of the "hypothesis-testing" approach must be kept in mind when results are interpreted.

The spectrum-fitting procedure begins with a trial model of the photon spectrum incident on the detector. The model is composed of a continuum of an assumed shape plus a number of narrow Gaussian-shaped lines superposed and is defined by an initial set of M parameters a_j ($j = 1, \ldots, M$). This photon model is folded through the instrument response to produce a corresponding count distribution, which is then compared with the observed background-subtracted distribution. We measure the quality of fit with the statistic s^2,

$$s^2 = \sum_i \left(\frac{c_i - m_i}{\sigma_i} \right)^2 ,$$

where c_i is the number of background-subtracted counts observed in detector channel i, m_i is the number of counts predicted by the model, and σ_i is the uncertainty associated with the number of counts. The statistic s^2 differs from the standard statistic, χ^2, in that the data are used to estimate this uncertainty rather than the model. To obtain the uncertainty estimate, we assume that the counts obtained from the flare and background observations are Poisson-distributed, so that the uncertainty associated with a channel is given by the square root of the number of counts observed. (The numbers of counts in all channels of interest here are sufficiently large to make this assumption reasonable.) Standard error propagation then provides the uncertainty estimate for the channels of the background-subtracted spectrum. We believe that this estimate is sufficiently accurate that the distribution of s^2 is negligibly different from that of χ^2. In the discussion that follows, therefore, we will refer to the statistic s^2 as χ^2.

The line and continuum parameters are then systematically varied, the modified model is folded through the instrument response, and a new χ^2 is calculated. This sequence is repeated until a best fit (i.e., minimum χ^2) is obtained. The nonlinear searching technique employed is the Levenberg-Marquardt method (e.g., see Press *et al.* 1988). This method uses a gradient-search technique far from minimum χ^2 and smoothly converts to an analytic technique as the minimum is approached. The analytic technique approximates the χ^2 function with an expansion to second order in the displacement of the parameters; this is equivalent to assuming that the χ^2 hypersurface is parabolic. Under this assumption, all necessary information about the hypersurface is contained in the "curvature matrix" α,

$$\alpha_{kl} \equiv \frac{1}{2} \frac{\partial^2 \chi^2}{\partial a_k \, \partial a_l} .$$

This matrix is calculated numerically by the fitting procedure.

The determination of uncertainties associated with the estimated parameters is discussed in some detail in the Appendix. For a parameter considered independently, the 1 σ (68.3%) confidence interval is given by that change from its best-fit value which produces a change in χ^2 of 1.0, all other parameters being adjusted to reminimize χ^2. As noted in the Appendix, to the extent that the χ^2 hypersurface projection for the given parameter is parabolic, the curvature matrix can be used to determine this uncertainty: it is simply the square root of the associated diagonal term of the inverse of the curvature matrix. Uncertainties calculated in this way are given in the tables below for all fitted parameters.

Confidence intervals obtained by using the covariance matrix are accurate for those parameters upon which the trial photon spectrum depends linearly (e.g., the intensities of the lines and continua), since the χ^2 surface projection for such parameters is, in fact, parabolic. However, the accuracy for nonlinear parameters can be very poor, depending on how far the true χ^2 surface projection for a given parameter deviates from parabolic. Precise uncertainties for such parameters can be obtained through explicit mapping of the χ^2 surface: the value of the parameter of interest is systematically displaced from its best-fit value and held fixed while the remaining parameters are optimized to reminimize χ^2. This is continued until $\Delta\chi^2 = 1.0$ is achieved. Such an analysis is CPU-time intensive, and we have performed it only for the line-center and width uncertainties of the photon model that provides the best fit to the data.

b) *Narrow-Line Modeling*

The actual profile of a gamma-ray line is not Gaussian. In fact, some lines can exhibit substantial structure (e.g., the 4.439 MeV line of ^{12}C; see Murphy, Kozlovsky, and Ramaty 1988). However, the accelerated-particle energy spectra in solar flares are, in general, sufficiently steep to result in line widths that are narrower than the *SMM*/GRS instrumental broadening. (For example, the expected width of the 4.44 MeV ^{12}C line is about 97 keV FWHM while the instrumental broadening at that energy is about 170 keV FWHM.) This substantial broadening, which is typical of NaI detectors such as the *SMM*/GRS, limits the detector's ability to determine the widths of such narrow lines. The use of Gaussian profiles to model such narrow gamma-ray lines is therefore generally adequate. This is not precisely true of the $\sim$0.45 MeV α-α line complex, which can have considerable structure depending on the angular distribution of the accelerated particles. This complex has been analyzed in detail by Murphy *et al.* (1990), where they conclude that the observed profile is best fitted by the single broad feature produced by an isotropic particle distribution. Using a Gaussian to represent this shape is reasonable.

While the Gaussian approximation may be adequate for modeling isolated gamma-ray lines, it may not be so for modeling a line which has nearby unresolved weak lines. Attributing the derived widths and line centers to the dominant line would not be correct. An example is the 6.129 MeV line from ^{16}O, produced predominantly by inelastic excitation of ^{16}O, and the 6.176 and 6.332 MeV lines from ^{15}O and ^{15}N, produced exclusively (in the solar atmosphere, that is) by spallation of ^{16}O. These spallation lines appear in Figure 1 as the high-energy shoulder on the 6.129 MeV ^{16}O line. For soft kinetic energy spectra the spallation lines are weak and the derived line parameters would essentially reflect the 6.129 MeV line itself. As the kinetic energy spectrum hardens, the spallation lines become more important; the apparent width of the line complex increases, and the apparent line center shifts to higher energies. The statistical quality of observed count distributions obtained from solar flares does not support the inclusion of any more than the strongest narrow lines in the line-fitting procedure, and no attempt has been made to decompose strongly blended lines into individual components. When interpreting the derived line-center energies and widths, these considerations must be remembered.

Inspection of the theoretical photon spectrum expected from solar flares (e.g., Fig. 1) and of the observed count distribution obtained from the 1981 April 27 flare (e.g., Fig. 4), suggests that the parameters of, at most, 10 narrow lines can be expected to be well determined by the fitting procedure. The nominal line energies for these 10 lines are 0.454, 0.511, 0.847, 1.238, 1.369, 1.634, 1.778, 2.223, 4.439, and 6.129 MeV, and Gaussians were assigned at these initial values. Three other narrow Gaussians were included in the fit. One Gaussian was assigned to each of the two complexes of narrow lines at $\sim$5.3 and $\sim$7.0 MeV which result primarily from inelastic excitation and spallation of ^{16}O. Since these Gaussians represent complexes, the derived line parameters have little direct meaning, and the Gaussians were included to improve the overall fit and to provide Compton-scattered counts in the lower channels. Last, a feature could be seen in the observed count distribution at $\sim$1.02 MeV, and a narrow Gaussian was assigned at that initial energy. Possible sources of such photons are spallation of ^{28}Si to give ^{27}Al$^{*1.014}$ and spallation of ^{12}C and ^{16}O to give

$^{10}B^{*1.023}$. Such lines are expected to be very weak, however. When the spectrum-fitting procedure is applied to flare data, the intensities, widths, and central energies of all of these 13 narrow lines are allowed to vary.

In solar flares the positron annihilation line (represented in the model by the Gaussian at 0.511 MeV) is expected to be accompanied by some amount of positronium continuum at photon energies below 0.511 MeV as discussed in § II. In an analysis (Murphy *et al.* 1990) of the nearby α-α feature in this flare, this continuum was shown to be weak compared with the α-α feature. No attempt has been made here to model such a continuum.

c) *Continuum Modeling*

A trial photon model in which the shape of the assumed total continuum which underlies the narrow lines is a simple power law would not be expected to provide a good fit to the observations. Although the spectrum of electron bremsstrahlung is quite possibly a power law, assuming such a shape for the total continuum would not account for the "nuclear continuum," which is quite different from a power law. As a test, a fit was attempted using a model composed of the above 13 narrow lines (with their central energies fixed at their theoretically expected values; see below) and a power-law continuum. The resulting χ^2 of 536.1 with 422 degrees of freedom corresponds to 0.014% confidence that such a model could have produced the observed data. A more complicated shape is clearly required to approximate better the actual total continuum spectrum. Here we proceed by assuming one of two basic continuum models. Model 1 is the sum of a power law,

$$\phi(\epsilon) = A_{\rm pl}(\epsilon/\epsilon_n)^{-s}\,, \qquad (1)$$

and an exponential spectrum,

$$\phi(\epsilon) = A_{\rm exp}(\epsilon/\epsilon_n)^{-1}\exp\,(-\epsilon/\epsilon_0)\,, \qquad (2)$$

where $\phi(\epsilon)$ is the fluence at photon energy ϵ (MeV) in units of photons cm^{-2} MeV^{-1}, and ϵ_n is an arbitrary normalizing energy; we take $\epsilon_n = 1$ MeV. In this model, the power law dominates at low energies and the exponential approximates the contribution of the "nuclear continuum" at higher energies. During the spectrum-fitting procedure, the intensities ($A_{\rm pl}$ and $A_{\rm exp}$), the power-law spectral index (s), and the exponential characteristic energy (ϵ_0) are varied. These four parameters plus those of the 13 narrow lines result in a total of 43 adjustable parameters for model 1.

In model 2 a more detailed modeling of the "nuclear continuum" is attempted. We have fitted the theoretical total "nuclear continuum" (the sum of the two lower curves shown in Fig. 1) with five broad Gaussians and found that a good fit could be obtained when these Gaussians were centered at 0.811, 1.515, 1.673, 4.267, and 5.931 MeV with respective FWHMs of 218, 759, 2749, 1350, and 3357 keV. (The best-fitting locations of these five lines suggest, as expected, that the lines are attempting to approximate the inverse-component structure due to reactions of accelerated Fe, Mg, Ne and Si, C, and O, respectively.) The model 2 continuum was then constructed using the power law of equation (1) plus these five broad Gaussians with their line centers and widths fixed at the above values. The intensities of the five Gaussians and of the power law, and the value of the power-law spectral index, are varied when the spectrum-fitting procedure is applied to flare data. These seven parameters plus those of the 13 narrow lines result in a total of 46 adjustable parameters for model 2.

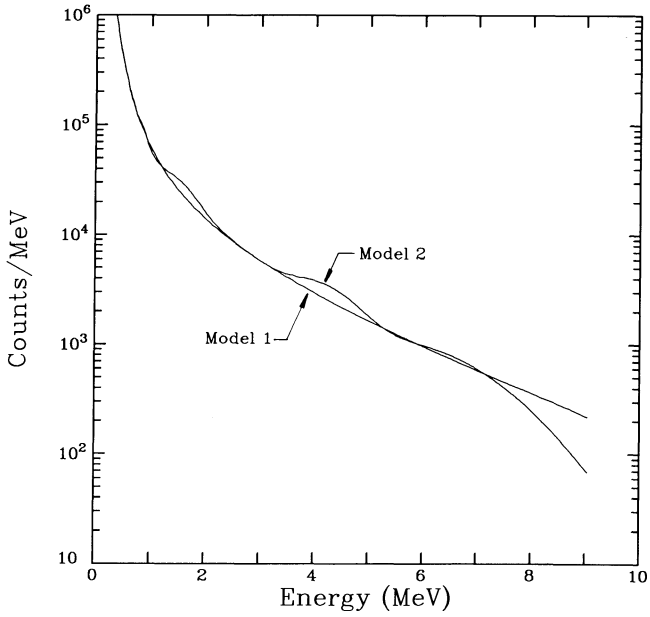

FIG. 3.—Comparison of the best-fitting continua of models 1 and 2

The essential difference between these two continuum models is the additional structure associated with model 2. This can be seen in Figure 3, where the two models are directly compared after they have been folded through the detector response; the spectral parameters generating the two models are the best-fitting values obtained below. The details of the differences will be discussed when the results of the line-fitting procedure are presented.

d) *Previous Analyses*

The *SMM*/GRS gamma-ray data from the 1981 April 27 flare has been analyzed previously, and we will compare the results derived here with the results of two of these previous analyses. We briefly describe these two techniques.

Using the detailed gamma-ray production theory of solar flares (e.g., Ramaty, Kozlovsky, and Lingenfelter 1979; Murphy 1985), Murphy *et al.* (1985*a*, *b*) developed a χ^2-minimization hypothesis-testing technique to determine the relative abundances of the ambient elements responsible for narrow-line production and applied the technique to the 1981 April 27 *SMM*/GRS gamma-ray data. Relative narrow-line intensities are not determined directly in the technique. Rather, individual theoretical gamma-ray spectra resulting from interactions of accelerated particles (with an assumed, fixed composition) with each of the various ambient elements in the solar atmosphere are calculated. The relative contribution of each is varied until the best fit to the data is obtained. Narrow-line intensities follow directly from the derived ambient abundances using the theoretically calculated line yields. Prompted by preliminary results from the present analysis, in which the strong effect of the underlying continuum on the derived narrow-line intensities (and thus, presumably, on the derived ambient abundances) was established, the abundance technique has been extended to determine the composition of the accelerated particles in addition to that of the ambient material. Details of the abundance technique and the full results of the analysis will be presented elsewhere. For comparison, we use here the narrow-line intensities implied by the

best-fitting model obtained with this extended abundance technique.

The abundance technique differs from the Gaussian-line technique developed in the present paper in several important ways:

1. In the Gaussian technique, the derived intensities of the various narrow lines are essentially independent of each other (except for a slight effect due to the Compton continuum from higher energy lines contributing to the underlying continuum). In the abundance approach, a given ambient element can contribute to several narrow lines with the relative contributions fixed by the nuclear cross sections for line production and the assumed accelerated-particle spectrum. The intensity ratio of two lines that are produced exclusively by only one ambient element is therefore completely fixed. However, the relative intensities of lines that are produced by more than one ambient element (via spallation from heavier elements in addition to direct excitation), as most are, vary as the abundances vary, but they are still considerably more constrained than in the Gaussian technique.

2. In the abundance technique, the shapes of the unresolved-line continua from each element heavier than O are fixed. They have been determined from laboratory measurements. These continua make significant contributions to the total "nuclear continuum."

3. In the abundance technique, the line centers, widths, and shapes are determined by the nuclear kinematics, cross sections, and the assumed accelerated-particle angular distribution.

In a separate previous analysis by Forrest and Murphy (1988), the central energies and widths of the three strongest narrow lines present in the count spectrum of the 1981 April 27 flare were determined. The analysis was performed by varying the parameters of a continuum functional form and of a Gaussian approximation for a line until the best fit to the data in a narrow region of the observed count spectrum around the line was obtained. The continuum functional form used was a representation of the instrumental response to assumed higher lying lines. The analysis used neither a hypothesis-testing nor a deconvolution technique. The lines were fitted using the count spectrum directly, and the derived widths therefore reflect not only the intrinsic line width but also the considerable broadening by the detector.

By comparing the narrow-line intensities derived under these various continuum assumptions, the additional uncertainty due to the incomplete knowledge of the true continuum shape can be estimated.

VI. RESULTS

We now discuss the results obtained in this present analysis and compare them with the results obtained in previous analyses. We discuss first the narrow-line parameters and then the time-dependent results.

a) Narrow-Line Parameters

Figures 4 and 5*a* show the observed count distribution obtained from the 1981 April 27 flare together with the best-fitting count spectrum derived using continuum models 1 and 2, respectively. The error bars associated with the data are statistical 1 σ. Also shown are the best-fitting total continuum, and the components comprising that continuum, for each model. For model 1 these components are the power law and the exponential. For model 2 they are the power law and the five broad Gaussians. Figures 5*b*–5*e* show the data and the fit of model 2 in greater detail with the best-fitting power law subtracted from both the data and the model to show the narrow-line structure more clearly.

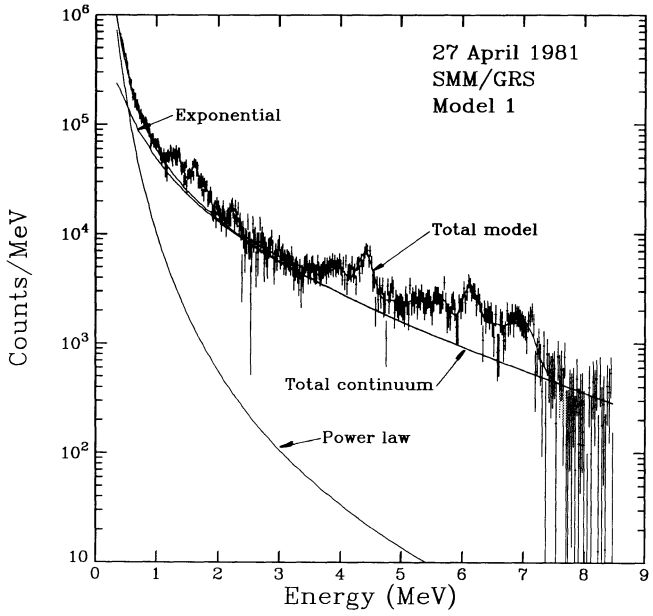

FIG. 4.—Gamma-ray data from the 1981 April 27 solar flare compared with the best-fitting spectrum of model 1. The vertical error bars associated with the data represent the propagated statistical uncertainties, and the horizontal error bars represent the bin energy width. The various components of the model are indicated.

For each model we present derived narrow-line intensities, centers, and widths and their associated 1 σ (i.e., $\Delta\chi^2 = 1.0$) uncertainties (as calculated analytically from the covariance matrix) in Tables 1, 2, and 3, respectively. The uncertainties obtained from the explicit χ^2 mapping for the line centers and widths derived under model 2 are also given in Tables 2 and 3 under the heading "map." As the widths of some of the lines of Table 2 were being systematically reduced during the mapping procedure, a change in χ^2 of 1.0 could not be achieved even though the width had been reduced to zero. The mapped lower-bound uncertainties shown in the table for such widths reflect this zero-width limit. The uncertainties obtained by explicit mapping were, in general, quite similar to those obtained directly from the covariance matrix, with some mapped values being somewhat larger. The mapping also revealed some unsymmetrical error limits.

i) *Narrow-Line Intensities*

The derived narrow-line intensities and associated uncertainties obtained under the two model assumptions are given in Table 1, the first column giving the nominal values for the line centers. At the bottom of the table are given the best-fitting power-law intensity (A_{pl}) and index (s) for both models and, for model 1, the exponential intensity (A_{exp}) and characteristic energy (ϵ_0). The continuum intensities are as defined in equations (1) and (2). The uncertainties for these continuum parameters are from the covariance matrix. Also given at the bottom of the table are the quality of fit as measured by χ^2, the number of degrees of freedom ν, and the probability $P(\chi^2)$ that a random observation of the true model could have produced an χ^2 as large or larger. A fit is considered acceptable if

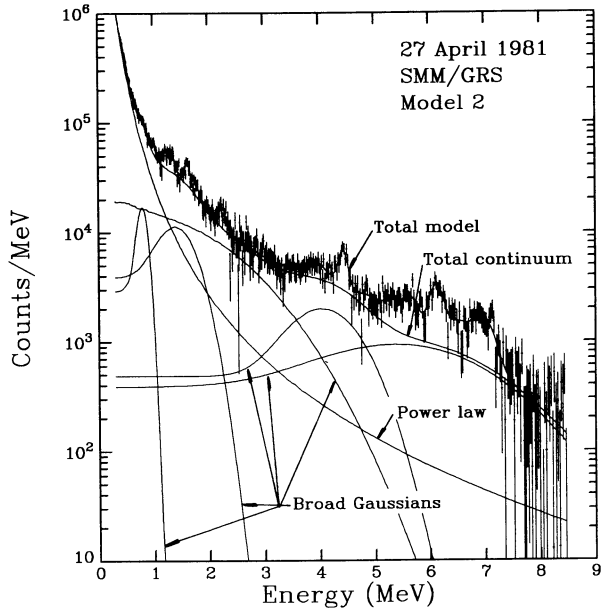

FIG. 5a

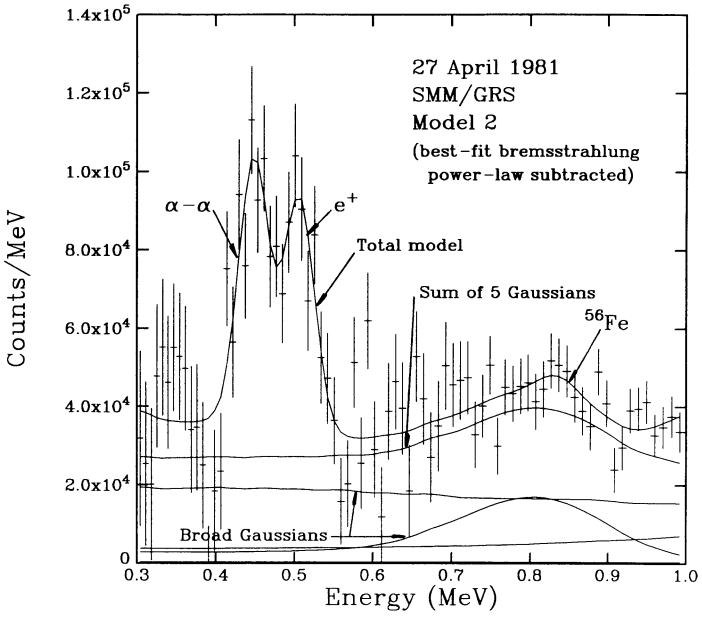

FIG. 5b

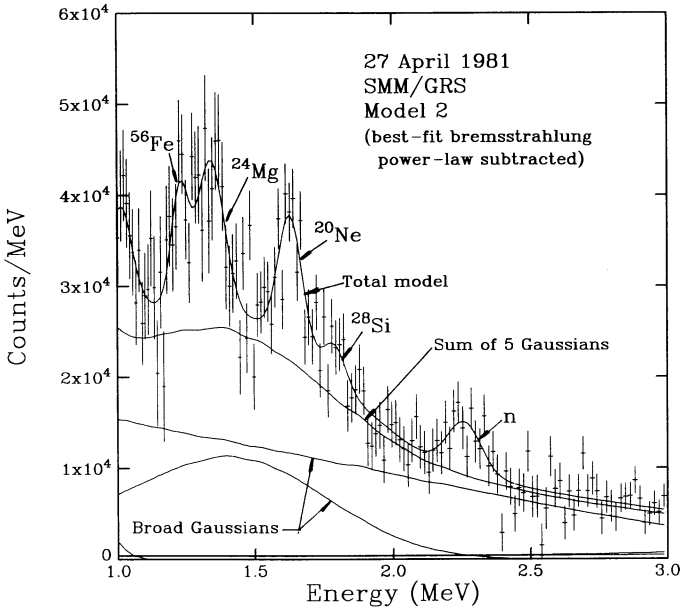

FIG. 5c

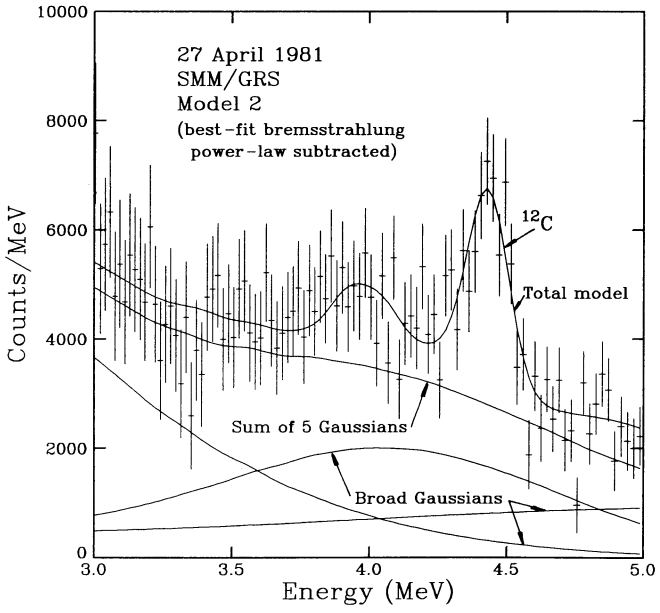

FIG. 5d

FIG. 5.—Gamma-ray data from the 1981 April 27 solar flare compared with the best-fitting spectrum of model 2. The various components of the model are indicated. Panels *b*–*e* (showing the fit with more detail) have the best-fitting power law subtracted from both the data and the model and have the nuclei responsible for the various narrow lines indicated (the ^{7}Li–^{7}Be complex is denoted by α-α, the positron-annihilation line by e^+, and the neutron-capture line by *n*).

$P(\chi^2) \simeq 0.50$. We note that the fitting technique failed to find a meaningful uncertainty for the weak 0.847 MeV line intensity in model 2.

We see that, while the model 1 continuum cannot be strongly rejected [$P(\chi^2) = 0.151$], the model 2 continuum clearly produces a much better fit [$P(\chi^2) = 0.565$]. This is due to the additional structure of model 2, which, while introducing more adjustable parameters and reducing the number of degrees of freedom, nevertheless improves the fit confidence level. We continue to use the results from model 1 for comparison in order to test the sensitivity of derived parameters to the underlying continuum assumption.

Table 1 shows that the derived best-fitting intensity for a given line can vary considerably under the two model assumptions. These differences are the direct result of the differences in structure between the two continuum models shown in Figure 3. In some energy ranges the model 1 continuum is the more intense of the two and in others model 2 is the more intense. But at every narrow-line location (except those of the 1.02 and 1.238 MeV lines) the model 2 continuum is the more intense

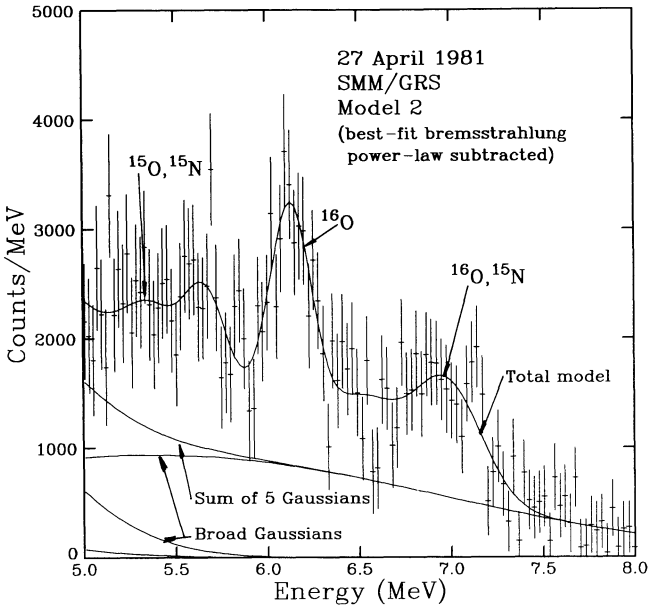

FIG. 5*e*

and, as a result, every line intensity (again, except those of the 1.02 and 1.238 MeV lines) derived using model 2 is less than when using model 1. In the 1.02 MeV region model 1 is higher and the derived intensity is lower. The 1.238 MeV line is located at an energy where the model continua are switching roles, and understanding the response of the fitting procedure is not as simple as in the other cases.

The results shown in Table 1 indicate that the derived values of the intensities of even strong, well-defined narrow lines can vary appreciably when the spectral shape for the underlying continuum is changed. For example, the best-fitting intensities for the 1.634 MeV line obtained with the two models changed by ~45%. Using the uncertainties from Table 1, the difference of the two intensity values differs from zero by ~2.4 σ. This corresponds to only a 1.5% chance that the two values could actually be the same. Additional uncertainty at this level due to insufficiently detailed knowledge of the true continuum shape does not appear in the statistically based uncertainties obtained by the fitting procedure. It should be noted, however, that if two different continuum models both produce acceptable fits to the data, then the derived uncertainties for any given parameter would be expected to be such as to make the two best-fitting values for the parameter consistent with each other. We explore the sensitivity of the derived narrow-line parameters to the underlying continuum more fully below.

TABLE 1

DERIVED LINE INTENSITIES (photons cm^{-2})

Nominal Line Energy (MeV)	Model 1[a]	Model 2[b]	Model 3[c]
0.454	29.3 ± 6.3	22.0 ± 4.7	27.5 ± 3.7
0.511	19.9 ± 5.0	20.3 ± 4.7	7.4 ± 1.9
0.847	4.8 ± 3.3	...[d]	5.5 ± 1.2
1.02	0.2 ± 30.5	9.0 ± 2.8	2.5 ± 0.6
1.238	4.9 ± 13.4	11.0 ± 5.6	6.1 ± 0.8
1.369	37.3 ± 16.8	22.8 ± 7.7	9.1 ± 2.0
1.634	40.2 ± 5.8	22.3 ± 4.6	21.8 ± 2.3
1.778	16.0 ± 4.9	7.5 ± 3.5	10.1 ± 1.6
2.223	15.8 ± 3.2	13.3 ± 3.1	6.2 ± 2.3
4.439	28.0 ± 2.0	17.0 ± 2.4	24.0 ± 2.6
~5.3	10.4 ± 1.8	8.9 ± 2.3	...
6.129	20.0 ± 1.7	19.6 ± 2.3	18.5 ± 1.3
~7.0	15.7 ± 1.7	15.1 ± 2.3	...
A_{pl} (photons MeV^{-1} cm^{-2})	89.9 ± 18.8	250.1 ± 14.4	236.6 ± 1.6
s	3.71 ± 0.12	2.97 ± 0.04	2.91 ± 0.03
A_{exp} (photons MeV^{-1} cm^{-2})	470.6 ± 92.2	...	...
ϵ_0 (MeV)	3.71 ± 0.29	...	...
χ^2	435.4	397.7	457.5
ν	406	403	427
$P(\chi^2)$	0.151	0.565	0.149

[a] Power law plus exponential.
[b] Power law plus five Gaussians.
[c] Abundance.
[d] Indeterminate. See text.

Narrow-line intensities can also be derived from the abundance-determining technique mentioned above. The implied line intensities, shown in the last colum of Table 1 and denoted model 3, can be significantly different from either model 1 or model 2. When the best-fitting total continuum (power law, unresolved component, and broad lines) resulting from the abundance technique is compared with that of models 1 and 2, the differences for each line can again be completely understood in terms of the different intensities of the total continuum underlying the lines.

We note that the best-fitting spectrum derived with the abundance technique does not provide as good a fit [$P(\chi^2) = 0.149$] as that of model 2 [$P(\chi^2) = 0.565$]. The abundance technique is heavily constrained by the assumptions mentioned above, and attempting to improve the fit by exploring the effect of varying these constrained parameters awaits future analysis. Detailed comparison of the acceptable fit obtained here with model 2 and the fit obtained by the abundance technique will give valuable insight on how the trial gamma-ray spectrum could be varied to improve the abundance fit.

ii) *Narrow-Line Centers*

Table 2 gives the center energies and associated uncertainties for the 13 narrow lines derived using continuum models 1 and 2. The fitting technique failed to obtain meaningful analytic uncertainties for the 1.02 MeV line in model 1 and the 1.02 and 1.238 MeV lines in model 2, suggesting that the actual χ^2 surface projection for these parameters deviates substantially from parabolic. Indeed, the mapped uncertainties for these parameters show considerable asymmetry. Also shown in the table are the values expected from isotropic interactions (referred to as "nominal" in the table), determined from the theoretically derived spectrum shown in Figure 1 that was calculated for a typical accelerated-particle kinetic energy spectrum. Except for the 1.778 and 2.223 MeV lines, all of the derived values are consistent (within ~1 σ) with the isotropic values. (Note: there are no well-defined line-center values for the 5.3 and the 7.0 MeV lines, since these are blends of several lines.) The 1.811 MeV line from ^{56}Fe could be shifting the fitted line center of the 1.778 MeV ^{28}Si line to higher energy. Similarly, the 2.22 MeV line is a blend of the 2.223 MeV neutron-capture line, the 2.231 MeV ^{32}S line, and the 2.313 MeV ^{14}N line. The neutron-capture line dominates for disk-centered flares but is strongly attenuated for limb flares such as that of 1981 April 27. This could explain the shift of the fitted center to higher energy. The derived line center of the 6.129 MeV ^{16}O

TABLE 2

DERIVED LINE CENTERS (MeV)

NOMINAL LINE ENERGY (isotropic)	MODEL 1[a]	MODEL 2[b]		FORREST AND MURPHY (1988)
		Analytic	Map	
0.454.....	0.446 ± 0.004	0.448 ± 0.004	$^{+0.004}_{-0.005}$	...
0.511.....	0.506 ± 0.004	0.507 ± 0.004	$^{+0.004}_{-0.004}$	...
0.847.....	0.829 ± 0.014	$0.834 \pm ...$[c]	$^{+0.039}_{-0.023}$	...
1.02.....	[c]	1.019 ± 0.012	$^{+0.012}_{-0.013}$	...
1.238.....	1.232 ± 0.038	$1.228 \pm ...$[c]	$^{+0.019}_{-0.007}$	...
1.369.....	1.350 ± 0.035	1.344 ± 0.016	$^{+0.012}_{-0.012}$	...
1.634.....	1.632 ± 0.008	1.635 ± 0.006	$^{+0.006}_{-0.006}$	1.628 ± 0.008
1.778.....	1.809 ± 0.016	1.795 ± 0.016	$^{+0.016}_{-0.022}$	...
2.223.....	2.259 ± 0.013	2.264 ± 0.014	$^{+0.014}_{-0.014}$	...
4.439.....	4.423 ± 0.010	4.436 ± 0.022	$^{+0.009}_{-0.013}$	4.430 ± 0.011
~5.3.....	5.339 ± 0.040	5.377 ± 0.047	$^{+0.065}_{-0.049}$	...
6.129.....	6.142 ± 0.013	6.143 ± 0.013	$^{+0.013}_{-0.013}$	6.147 ± 0.022
~7.0.....	6.984 ± 0.030	6.995 ± 0.032	$^{+0.032}_{-0.031}$	...

[a] Power law plus exponential.
[b] Power law plus five Gaussians.
[c] Indeterminate. See text.

TABLE 3

DERIVED LINE WIDTHS (FWHM in keV)

NOMINAL LINE ENERGY (MeV)	MODEL 1[a]	MODEL 2[b]		THEORY
		Analytic	Map	
0.454.....	34 ± 16	23 ± 18	$^{+13}_{-11}$	84
0.511.....	16 ± 30	21 ± 24	$^{+18}_{-21}$	<10
0.847.....	...[c]	$5 \pm ...$[c]	$^{+75}_{-5}$	5
1.02.....	...[c]	60 ± 41	$^{+48}_{-60}$	30
1.238.....	...[c]	$5 \pm ...$[c]	$^{+58}_{-5}$	7
1.369.....	163 ± 81	88 ± 52	$^{+57}_{-51}$	15
1.634.....	118 ± 29	55 ± 35	$^{+54}_{-55}$	22
1.778.....	85 ± 56	$26 \pm ...$[c]	$^{+90}_{-26}$	20
2.223.....	106 ± 48	84 ± 56	$^{+41}_{-49}$	...
4.439.....	193 ± 28	$19 \pm ...$[c]	$^{+70}_{-19}$	97
~5.3.....	298 ± 92	311 ± 111	$^{+137}_{-209}$	...
6.129.....	172 ± 40	172 ± 45	$^{+46}_{-48}$	114
~7.0.....	349 ± 71	357 ± 80	$^{+86}_{-63}$	...

[a] Power law plus exponential.
[b] Power law plus five Gaussians.
[c] Indeterminate. See text.

line, while consistent with the isotropic value, is somewhat high, perhaps because of the 6.176 and 6.332 MeV ^{16}O spallation lines discussed above. The derived centers for the 1.634, 4.439, and 6.129 MeV lines are also consistent with the values derived by Forrest and Murphy (1988) for this flare, shown in the last column of Table 2.

iii) *Narrow-Line Widths*

Table 3 gives the line widths (FWHM) and uncertainties for the narrow lines derived using models 1 and 2. The fitting technique failed to obtain meaningful analytic uncertainties for the weak 0.847, 1.02, and 1.238 MeV lines in model 1 and the 0.847 and 1.238 MeV lines in model 2. Sensitivity to the assumed underlying continuum, similar to that found above for the intensities, is found for the widths as well. In general, when the underlying continuum is reduced, the fitting procedure attempts to compensate by broadening the fitted line width and increasing the fitted intensity. Comparing models 1 and 2 in Tables 1 and 3, we see that whenever the intensity of a line is relatively high (implying a relatively low underlying continuum), its width is, in general, correspondingly broader.

The derived widths can be compared with what would be expected from a typical solar flare. As discussed above, line widths can have some dependence on the accelerated-particle kinetic energy spectrum and angular distribution. Shown in the last column of Table 3 are the narrow-line widths expected from isotropic interactions of accelerated particles having a Bessel function spectrum with $\alpha T = 0.025$. Murphy *et al.* (1990), in their analysis of the ~0.450 MeV α-α line complex, found the data to be consistent with an isotropic distribution of the α-particles. A spectral index of $\alpha T = 0.025$ is typical of the values derived for a number of flares from the observed ratio of the 2.223 MeV neutron-capture line fluence and the 4–7 MeV nuclear fluence (see Ramaty and Murphy 1987). The widths shown in the table were determined by fitting Gaussians to the narrow lines in the theoretically derived spectrum shown in Figure 1. The underlying continuum in this case is well defined and should contribute minimal uncertainty to the results. The width of the 2.223 MeV neutron-capture line is expected to be less than 100 eV, but we do not include this in Table 3, since the fitted width depends on the strengths of the close-lying 2.231 MeV ^{32}S and 2.313 MeV ^{14}N lines, which, for this limb flare, are relatively strong. Similarly, the ~5.3 and ~7.0 MeV lines are blends, and their widths are not given.

The best-fitting widths derived assuming either model 1 or model 2 are, in general, broader than the expected widths calculated under the assumptions stated above, although the associated uncertainty in some cases makes the values consistent. These differences are, again, directly related to the strength of the underlying continuum and are consistent with the generally higher intensities of the lines derived using models 1 and 2 relative to those of the abundance determination. This sensitivity is explored further below.

Finally, the derived widths can be compared with those determined by Forrest and Murphy (1988) for the 1.634, 4.439, and 6.129 MeV lines. This comparison, however, is not direct, since Forrest and Murphy derived the line widths as they appeared in the count distribution, and such widths include the additional broadening produced by the instrumental response. The widths derived in the present paper are for the incident

gamma-ray line before instrumental broadening. Forrest and Murphy found 113 ± 14, 170 ± 26, 177 ± 40 keV (FWHM), respectively, for the instrumentally broadened lines. They compared these widths with those due to the instrument itself (88, 170, and 221 keV, respectively) and concluded that the derived widths were consistent with actual line widths much narrower than those due to instrumental broadening. The widths derived here for model 2 are reasonably consistent with those derived by Forrest and Murphy; simple adding in quadrature with the instrumental broadening gives 104 ± 19, 171 ± 24, and 280 ± 28 keV, respectively. The widths derived for model 1, however, are somewhat broader: 147 ± 23, 257 ± 21, and 280 ± 25 keV. These differences can again be accounted for by the level of the underlying continuum established by the fit. The widths derived here result from optimizing the fit over the full usable detector energy range of 0.3–8.5 MeV with the assumed continuum model. Forrest and Murphy used a continuum shape derived from the instrument response due to higher lying lines and optimized the fit over a narrow range around the line being fitted. The two techniques obtain different continuum intensities under the lines, and different widths necessarily result.

iv) *Narrow-Line Parameter Discussion*

We explore the sensitivity of the derived intensities and widths to the level of the underlying continuum by investigating the 4.439 MeV line in some detail. The data near the line were fitted with a Gaussian plus a continuum, the fit being optimized over the narrow range of 3.5–5.5 MeV. For simplicity, the continuum was chosen to be a simple power law. The best-fitting line width (FWHM) and intensity were 56 ± 50 keV (instrumentally broadened to 179 ± 16 keV) and 15.9 ± 1.6 photons cm^{-2}, respectively. The width is consistent with theory, the Forrest and Murphy result, and the model 2 results above. We then reduced the continuum intensity by 5%, held it fixed at that level, and refitted the line. We then found a width of 108 ± 34 keV (an increase of 92%) and an intensity of 18.1 ± 1.3 photons cm^{-2} (an increase of 14%). Figures 6 and 7 show the resulting fits with χ^2 increasing from 76.4 to 79.8, which, for 88 and 90 degrees of freedom, corresponds to confidence levels of 0.81 and 0.77, respectively. While the fitted width has increased considerably, both fits are equally acceptable. Uncertainties in knowledge of the detailed structure of the continuum on the order of 5% in a particular region certainly would not be surprising. The best-fitting values for the widths are clearly very sensitive to the level of the underlying continuum.

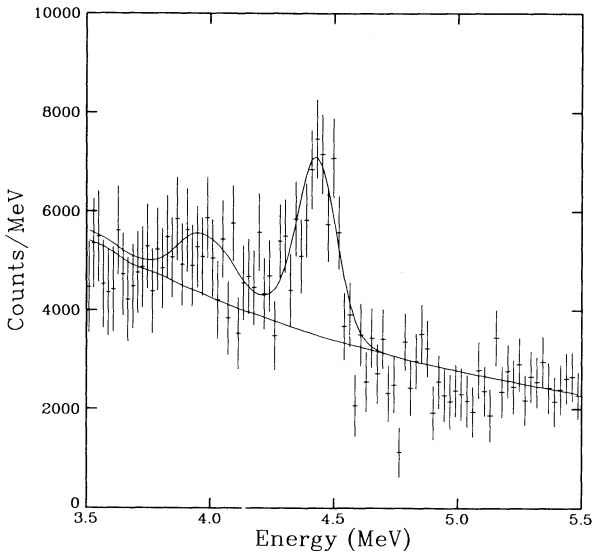

FIG. 6.—Full fit to the 4.439 MeV line over the range 3.5–5.5 MeV assuming a power-law continuum.

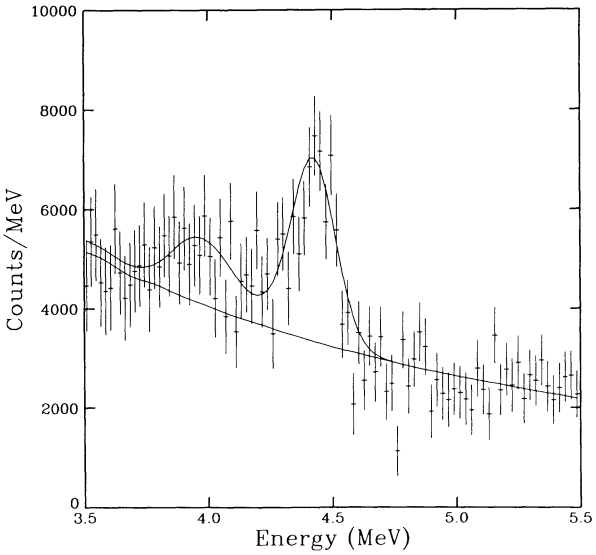

FIG. 7.—Same as Fig. 6, but with the continuum reduced by 5% from its best-fitting value as shown in Fig. 6.

It should be noted that, although the specific, best-fitting values are substantially different, the associated uncertainties are such as to make the two values statistically consistent (the difference of the two values differs from zero by only 0.9 σ—i.e., they are, in fact, equal at a 37% confidence level). This should also be true for any parameter derived from models which both produce acceptable fits to the data. Lampton, Margon, and Bowyer (1976) emphasize that "it is the *range* of parameter values to which a theory is restricted that is the useful result of an experiment. The discrete best-fitting values of the parameters are essentially statistical artifacts."

b) Time-dependent Results

We now investigate how the total nuclear and integrated electron emissions varied as the flare progressed. Because the model 2 continuum is based on the well-established theory of gamma-ray production in solar flares, we believe that it represents a good approximation to the actual continuum observed from flares. The fact that it provides a good fit to the data supports this belief. Therefore, while some individual narrow-line parameters may still be sensitive to the precise level of the underlying continuum, the total nuclear emission, defined in model 2 as the sum of the intensities of all lines (the narrow lines plus the five broad lines), should be reasonably well determined. (We do not include the 0.51 and 2.2 MeV lines, since the annihilation and neuturon-capture lines have much longer emission time profiles than those of the de-excitation lines.) Similarly, to the extent that the electron bremsstrahlung spectrum is an unbroken power law, the integrated bremsstrahlung emission should also be reasonably well determined.

The best-fitting power-law parameters derived here for

model 2 can be compared with the results of Vestrand *et al.* (1987), where the *SMM*/GRS data for a number flares were analyzed. In the analysis, the observed gamma-ray spectra were fitted with a power law of the form of equation (1), and no attempt was made to correct for any effect due to the presence of nuclear emission in this energy range. Such an effect is expected to be small, however. The power-law amplitude derived for the 1981 April 27 flare cannot be compared with the amplitude obtained in the present analysis because Vestrand *et al.* do not indicate their flare integration duration. The power-law index obtained for the flare was 2.7 ± 0.1, which is a somewhat harder index than that derived here (2.94 ± 0.04). This difference could be due to the nuclear emission, which would be expected to harden the fitted power law if not accounted for.

Using the results of model 2, we find that the total time-integrated fluence in the 4.1–6.4 MeV "main-channel window" was 111.3 ± 2.2 photons cm^{-2} and that the portion of this due to nuclear emission was 106.7 ± 2.1 photons cm^{-2}, confirming that the emission in this energy range is dominated by the nuclear component (see Ramaty, Kozlovsky, and Suri 1977; Ibragimov and Kocharov 1977).

We now analyze each of the maximum and minimum subintervals defined in § IV above with a simplified version of the fitting technique using continuum model 2. Both the central energies and the widths of the narrow and broad lines were held fixed at the best-fitting values previously obtained by fitting the total flare. Only the intensities of the lines and the power law and the power-law spectral index were allowed to vary during the fitting procedures. Acceptable fits were achieved, with reduced χ^2, $\chi^2_\nu = \chi^2/\nu$, varying between 0.92 and 1.18 for the 403 degrees of freedom. We obtain average fluxes for each interval by dividing the best-fitting time-integrated fluence for each by the corresponding detector live time (see § IV). The results of this analysis are shown in Figures 8–11, where the vertical error bars represent the statistical uncertainties obtained from the covariance matrix and the horizontal error bars represent the interval integration time.

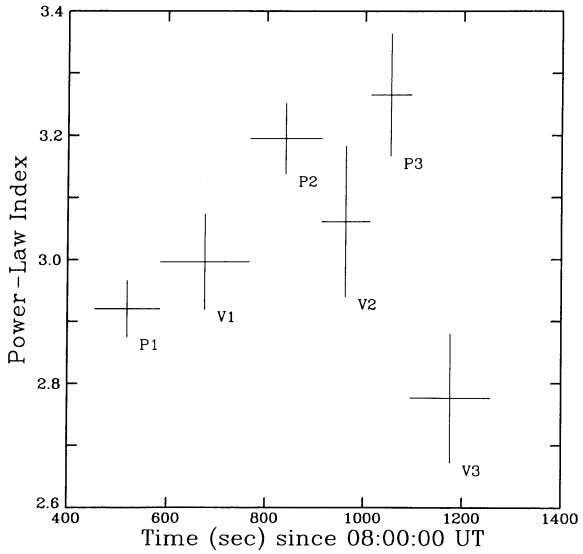

FIG. 9.—Best-fitting bremsstrahlung power-law indices for the six flare subintervals.

We first consider the bremsstrahlung power-law parameters. The best-fitting fluxes of the integrated bremsstrahlung emission above 0.3 MeV for the six intervals are given in Figure 8, showing that the intensity generally decreases as the flare progresses. The six corresponding best-fitting power-law indices are shown in Figure 9. No significant evolution of the index with time is present (46% confidence that the index is not linearly correlated with time), although the data are not consistent with a constant value (<0.01% confidence level). The data for the three maximum intervals were then summed together, as were the three minimum intervals, to obtain total maximum and total minimum spectra, respectively, and the simplified fitting procedure was applied to each. The values for the integrated bremsstrahlung flux above 0.3 MeV during the summed maximum and summed minimum intervals were 1.742 ± 0.159

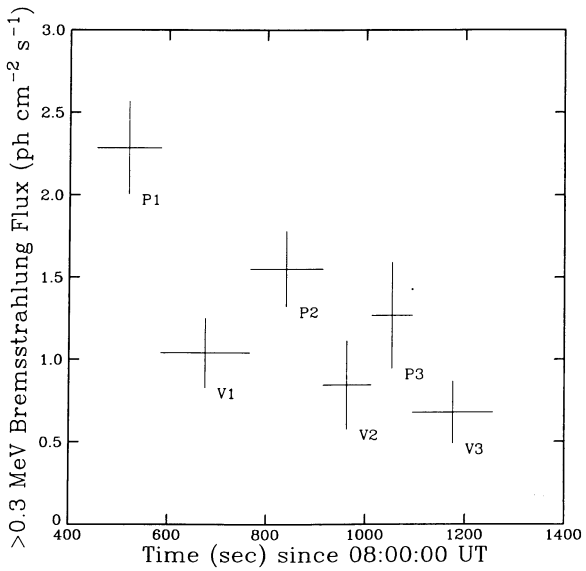

FIG. 8.—Best-fitting fluxes of the integrated bremsstrahlung power-law emission above 0.3 MeV for the six flare subintervals.

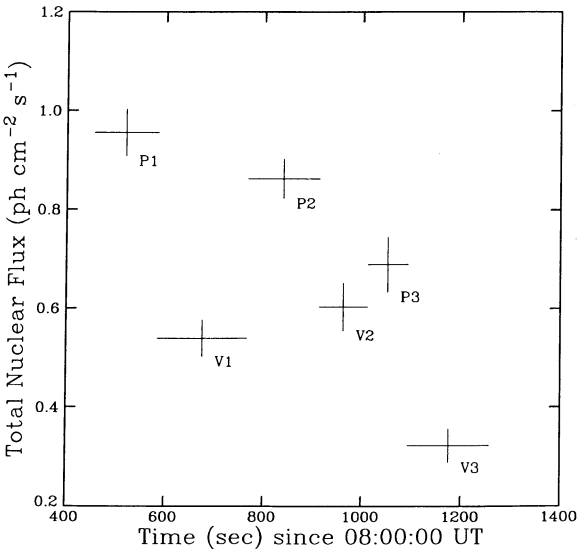

FIG. 10.—Best-fitting total nuclear emission fluxes for the six flare subintervals.

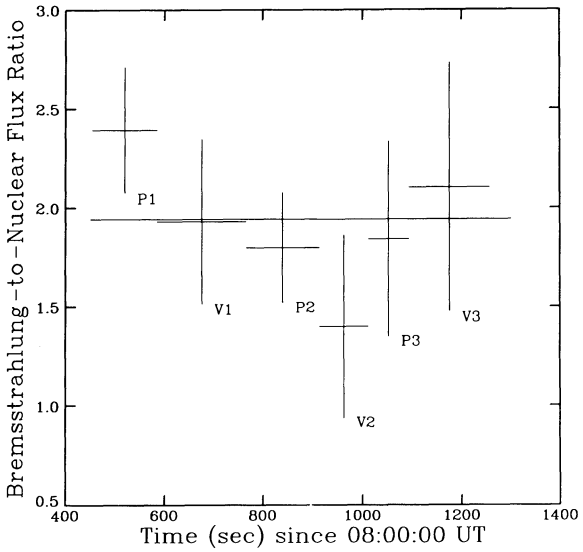

FIG. 11.—Ratio of the integrated bremsstrehlung emission above 0.3 MeV to the total nuclear emission for the six flare subintervals.

and 0.857 ± 0.124 photons cm^{-2} s^{-1}, respectively. The best-fitting values of the spectral indices were 3.08 ± 0.04 and 2.94 ± 0.05, respectively. The difference of the two flux values differs from zero by 4.4 σ, indicating that they are to be considered different at a high confidence level. The difference of the two index values differs from zero by 2 σ, indicating that, if they are to be considered different, they are so only at the 96% confidence level. Apparently the variation of the index throughout the flare cannot be simply attributed to differences in the spectra present during the maximum periods and during the minimum periods.

The best-fitting total nuclear emission fluxes for the six time intervals are shown in Figure 10. This flux also shows an overall decrease as the flare proceeds. Unfortunately, we can say nothing about the shape of the kinetic energy spectrum of the accelerated protons and nuclei as we could about the electron spectrum. No sufficiently sensitive indicator appropriate for the time resolution of ~ 100 s associated with the maximum and minimum intervals of this flare is available. (The traditional measure of nuclear spectral shape, the ratio of the 2.223 MeV neutron-capture line fluence to the de-excitation line fluence in the 4–7 MeV band, cannot be used, since it requires integrating the 2.223 MeV flux over a much longer time interval.) We therefore can say nothing about any possible correlation between the shapes of the energy spectra of the accelerated electrons and the accelerated nuclei.

A quantity of particular interest is the ratio of the bremsstrahlung above 0.3 MeV to the total nuclear emission. This ratio, which gives a measure of the relative strength of the acceleration and/or interaction of electrons versus nuclei, is shown in Figure 11 for the six time intervals. The values are consistent with a constant value of 1.94 ± 0.39 at a 58% confidence level (also shown in Fig. 11). In addition, the ratios obtained from the summation of the three maximum periods and from the summation of the three minimum periods are 1.99 ± 0.19 and 1.77 ± 0.27, respectively. The difference of these two values differs from zero by 0.7 σ, implying that they are the same at a 50% confidence level.

VII. SUMMARY

We have determined the intensities, line centers, and widths of the 13 strongest narrow lines appearing in the observed count spectrum of the 1981 April 27 solar flare. The fitting technique used optimized the fit of a model spectrum to the data by systematically varying the parameters of the model spectrum to minimize a χ^2-like statistic. The model spectra were composed of an underlying continuum of an assumed shape with narrow, Gaussian-shaped lines superposed. We list the important conclusions and then discuss each point more fully. We found the following:

1. The gamma-ray continuum underlying the narrow lines cannot be modeled solely with a power law, since this does not account for the nuclear emission that is not confined to the narrow lines.

2. To achieve an acceptable fit to the data, this additional "nuclear continuum" must be modeled with more structure than simple shapes can provide.

3. While the narrow-line centers are well determined, both the line intensities and the line widths can vary considerably as the underlying continuum model is changed.

4. Using a "nuclear continuum" model that is based on theoretical considerations and that provides a good fit to the data, we find that, while the emission attributed to nuclear interactions and the emission attributed to electron interactions varied considerably as the flare progressed, the ratio of these two emissions was consistent with a constant value of 1.94 ± 0.39 throughout the flare.

We have shown that a continuum which is composed only of a power law cannot account for the gamma-ray emission of this flare, which is neither due to electron interactions nor present in the narrow lines. A more complicated shape is required to account for this additional emission which is due to (1) nuclear interactions involving accelerated nuclei heavier than He and (2) the "continuum" of weak, narrow lines from excited nuclei heavier than oxygen, which are unresolvable with NaI detectors such as that of the *SMM*/GRS.

We investigated two basic continuum shapes. Model 1 was composed of a power law plus an exponential shape to approximate the additional nuclear continuum emission. Model 2 was composed of a power law plus five broad Gaussians for the nuclear continuum. The line centers and widths of the broad Gaussians were established by fitting Gaussians to theoretically derived solar flare gamma-ray spectra. The essential difference between the two continua is the additional structure associated with model 2. During the fitting procedure, the intensities, line centers, and widths of all narrow lines and the power-law intensity and index were varied for both models. In addition, the intensity and characteristic energy of the exponential of model 1 and the intensities of the broad Gaussians of model 2 were varied.

We found that the model 2 continuum gave an acceptable fit to the data but that the model 1 fit was not as good. The additional structure associated with model 2 was better able to reproduce the structure of the actual "nuclear continuum" produced by the flare. We found further that, while the derived line centers were well determined, both the derived intensities and widths varied appreciably when the continuum model was changed. This variation was seen to be a direct result of the level of the continuum underlying the line. In general, when the continuum under a given line is lowered, the line intensity and width both increase. The response of fitted parameters to the

continuum level can be quite strong; for example, the fitted width of the 4.439 MeV line increased by 92% when the continuum level was reduced by only 5%. If the energy dependence of the continuum is thought to be very smooth, determining parameters for the various lines by fitting only over a narrow region of the data around each line could give erroneous results, since a concatenation of the continuum sections resulting from the various individual line fits would not, in general, be smooth. A simultaneous fitting of all of the lines with a continuum model possessing sufficient, adjustable structure is preferred.

We compared the results with results from an abundance determination using data from this flare and an extension of the technique developed by Murphy *et al.* (1985*a*, *b*). Differences in parameter values derived by the various techniques could again be understood completely in terms of the level of the underlying continuum. The fit obtained using the model 2 continuum was, in fact, better than that of the highly constrained abundance determination. The model 2 best-fitting photon spectum will be invaluable as a guide to how the physical parameters defining the theoretical spectra used in the abundance technique should be varied to improve that fit.

We believe that using the model 2 continuum, which not only provides an acceptable fit but is constructed of components which are chosen to represent specifically and accurately the electron emission and the "nuclear continuum" emission, results in a reliable separation of the total electron contribution and the total nuclear contribution. Using the results of model 2, we find that the total time-integrated fluence in the 4.1–6.4 MeV "main-channel window" was 111.3 ± 2.2 photons cm^{-2} and that the portion of this to be attributed to nuclear emission was 106.7 ± 2.1 photons cm^{-2}, confirming that emission in this energy range is dominated by the nuclear component.

Using model 2, we have also investigated how the nuclear and electron emissions varied as the flare progressed. We found that the power-law index exhibited significant variation during the flare, but that this variation could not be attributed to any difference between the summed maximum and summed minimum emission periods. We also found that, while both the electron bremsstrahlung and the nuclear emission varied considerably as the flare progressed, the ratio of bremsstrahlung to nuclear emission was consistent with a constant value. The near-constancy of this ratio suggests that the nuclei and electrons in this flare were accelerated by common or related mechanisms.

The set of continuum and line parameters derived here for the 1981 April 27 flare provides a baseline with which results obtained from other flare data can be compared when such data are analyzed in a similar manner. Data with good statistical significance from a number of flares already exist in the *SMM* data base, and additional *SMM* data are anticipated from flares expected to occur as the next solar maximum develops. While values for some individual line parameters may be uncertain as we show here, their relative variation from flare to flare can nevertheless give valuable insight into the nature of high-energy processes occurring in flares. Also, when the continuum model used is constructed of components chosen to represent accurately the expected continuum from solar flares, the total nuclear and the total electron emissions can be comparatively well determined. These emissions provide a measure of a fundamental property of the acceleration process: the relative efficiency of proton and electron acceleration. The technique developed here provides a simple and efficient analytic tool that can be used for the statistical analysis of data from a large number of flares.

APPENDIX

CONFIDENCE LIMITS ON ESTIMATED MODEL PARAMETERS

What is needed to characterize precisely uncertainties associated with a number M of fitted parameters (denotes by the vector $\boldsymbol{a}_0$) obtained from a measured data set (denoted by D_0) is the probability distribution for the occurrence of the quantity $\boldsymbol{a}_i - \boldsymbol{a}_{\rm true}$, where the $\boldsymbol{a}_i$ are the parameter sets obtained by fitting a large number of data sets D_i imagined to be generated from the set of actual parameters $\boldsymbol{a}_{\rm true}$, which are unknown. Since this distribution is not available, we assume that the quantity $\delta\boldsymbol{a} \equiv \boldsymbol{a}_i - \boldsymbol{a}_0$ is distributed nearly the same as $\boldsymbol{a}_i - \boldsymbol{a}_{\rm true}$. This approximate distribution can be generated by fitting a large number of synthetic data sets constructed from D_0 using random numbers and plotting the resulting $\boldsymbol{a}_i - \boldsymbol{a}_0$ in the M-dimensional parameter space.

A confidence region is a region of this space containing a given fraction of the parameter sets. The shape of this confidence region is not constrained, but, when the method used to estimate the parameters is χ^2 minimization, there is a natural choice. The value of χ^2 is minimum at the best-fitting parameter set $\boldsymbol{a}_0$ (call this value $\chi^2_{\rm min}$) and increases as $\boldsymbol{a}$ is perturbed away from $\boldsymbol{a}_0$. The region within which χ^2 increases by no more than a given amount $\Delta\chi^2$ defines an M-dimensional confidence region around $\boldsymbol{a}_0$.

If one is not interested in the full M-dimensional confidence region but in a confidence region for some smaller number ν of "interesting" parameters, the natural confidence region in the ν-dimensional subspace of the M-dimensional parameter space is the projection of the M-dimensional region defined by a given $\Delta\chi^2$ into the ν-dimensional subspace of interest. A theorem (see Press *et al.* 1988) connects the projected confidence region with a confidence level. In principle, this theorem holds only when the measurement errors are normally distributed (which is assumed to be the case here) and either (1) the model is linear in all parameters or (2) the parameter uncertainties do not extend outside a region in which the model could be replaced by a linear model. Unfortunately, the model used here is nonlinear and may not meet the second requirement. However, Lampton, Margon, and Bowyer (1976) have used numeric simulations to conclude that there is no evidence of any departure of the actual uncertainties from those predicted by the theorem regardless of the degree of nonlinearity introduced.

The theorem states: "Suppose ν parameters are held fixed and the remaining $M - \nu$ parameters are varied to reminimize χ^2. Call this new minimum value $\chi^2(\nu)$. Then $\Delta\chi^2 \equiv \chi^2(\nu) - \chi^2_{\rm min}$ is distributed as χ^2 with ν degrees of freedom." For example, for $\nu = 1$ the projected subspace is the axis of the parameter of interest and $\Delta\chi^2 = 1.0$ for a 1 σ (68.3%) confidence region. For $\nu = 2$ the

projection is a region in the associated plane and $\Delta\chi^2 = 2.30$ for a 1 σ confidence region. For $\nu = 3$ the subspace is a three-dimensional volume and $\Delta\chi^2 = 3.53$ for 1 σ. The meaning of these 1 σ confidence regions is that 68.3% of all possible parameter sets contain parameter subsets whose ν-values fall within the projected region. The remaining $M - \nu$ parameters might differ from their best-fitting values by any amount. For $\nu > 2$ the confidence regions cannot be presented in any reasonable form. For this reason, the parameter uncertainties given in this paper are the 1 σ (68.3%) values calculated for $\nu = 1$, i.e., $\Delta\chi^2 = 1.0$. For those parameter subsets which, because of strong correlations among them, should always be simultaneously considered, this procedure may underestimate the uncertainties somewhat, but the only accurate representation of the confidence region is the multidimensional projected volume, which cannot be presented.

Creating the approximation to the parameter-space probability distribution by using random numbers to generate data sets from the observed data set and fitting each of them is impractical. We can, however, explore limited regions of this distribution relatively efficiently. To the extent that the χ^2 hypersurface is parabolic in $\delta\boldsymbol{a} \equiv \boldsymbol{a} - \boldsymbol{a}_0$, the curvature matrix $\boldsymbol{\alpha}$,

$$\alpha_{kl} \equiv \frac{1}{2}\frac{\partial^2\chi^2}{\partial a_k \partial a_l},$$

can be used. The equation for the boundary of a desired confidence region in the ν-dimensional subspace of interest is given by (Press *et al.* 1988)

$$\Delta\chi^2 = \delta\boldsymbol{a} \cdot (\mathbf{C}_{\text{proj}})^{-1} \cdot \delta\boldsymbol{a},$$

where the matrix $\mathbf{C}_{\text{proj}}$ is the $\nu \times \nu$ intersection of the ν rows and columns of the $M \times M$ matrix $\mathbf{C} \equiv \boldsymbol{\alpha}^{-1}$ corresponding to the parameters of interest. For $\nu = 1$, the solution of this equation is $\delta a_i = \pm(\Delta\chi^2 C_{ii})^{1/2}$, where a_i is the parameter of interest. For a 1 σ confidence level, $\Delta\chi^2 = 1.0$ and the uncertainty is then simply given by the square root of the associated diagonal term of the inverse of the curvature matrix.

REFERENCES

Craig, I. J. D., and Brown, J. C. 1986, *Inverse Problems in Astronomy* (Bristol: Hilger).
Forrest, D. J., *et al.* 1980, *Solar Phys.*, **65**, 15.
Forrest, D. J., and Murphy, R. J. 1988, *Solar Phys.*, **118**, 123.
Ibragimov, I. A., and Kocharov, G. E. 1977, *Soviet Astr. Letters*, **3** (No. 5), 221.
Kozlovsky, B., and Ramaty, R. 1977, *Ap. Letters*, **19**, 19.
Lampton, M., Margon, B., and Bowyer, S. 1976, *Ap. J.*, **208**, 177.
Letaw, J. R., Share, G. H., Kinzer, R. L., Silberberg, R., Chupp, E. L., Forrest, D. J., and Rieger, E. 1989, *J. Geophys. Res.*, **94**, 1211.
Meyer, J. P. 1985, *Ap. J., Suppl.*, **57**, 173.
Murphy, R. J. 1985, Ph.D. thesis, University of Maryland.
Murphy, R. J., Forrest, D. J., Ramaty, R., and Kozlovsky, B. 1985*a*, *Proc. 19th Internat. Cosmic Ray Conf.*, **4**, 253.
Murphy, R. J., Hua, X.-M., Kozlovsky, B., and Ramaty, R. 1990, *Ap. J.*, **351**, 299.
Murphy, R. J., Kozlovsky, B., and Ramaty, R. 1988, *Ap. J.*, **331**, 1029.
Murphy, R. J., Ramaty, R. Forrest, D. J., and Kozlovsky, B. 1985*b*, *Proc. 19th Internat. Cosmic Ray Conf.*, **4**, 249.
Press, W. H., Flannery, B. P., Teukolsky, S. A., and Vetterling, W. T. 1988, *Numerical Recipes* (Cambridge: Cambridge University Press).
Ramaty, R., and Crannell, C. J. 1976, *Ap. J.*, **203**, 766.
Ramaty, R., Kozlovsky, B., and Lingenfelter, R. E. 1979, *Ap. J. Suppl.*, **40**, 487.
Ramaty, R., Kozlovsky, B., and Suri, A. N. 1977, *Ap. J.*, **214**, 617.
Ramaty, R., and Murphy, R. J. 1987, *Space Sci. Rev.*, **45**, 213.
Share, G. H., Kinzer, R. L., Strickman, M. S., Letaw, J. R., Chupp, E. L., Forrest, D. J., and Rieger, E. 1989, *AIP Conf. Proc. 186, High Energy Radiation Background in Space* (New York: AIP), p. 266.
Vestrand, W. T., Forrest, D. J., Chupp, E. L., Rieger, E., and Share, G. H. 1987, *Ap. J.*, **322**, 1010.

DAVID J. FORREST: Department of Physics and Astronomy, University of New Hampshire, Durham, NH 03824

JOHN R. LETAW: Severn Communications Corporation, 223 Benfield Park Drive, Millersville, MD 21108

RONALD J. MURPHY and GERALD H. SHARE: E. O. Hulburt Center for Space Research, Naval Research Laboratory, Washington, DC 20375